JOURNAL OF AIRCRAFT
Vol. 45, No. 5, September–October 2008

Flow Measurements in a Short Takeoff, Vertical Landing Fountain: Parallel Jets

A. J. Saddington,* K. Knowles,† and P. M. Cabrita‡
Cranfield University, Shrivenham, England SN6 8LA, United Kingdom

DOI: 10.2514/1.32599

The interaction of multiple jets with the ground is of great importance for the design and operation of short takeoff, vertical landing aircraft. The fountain upwash flow, generated by the impingement of two axisymmetric, compressible, turbulent jets onto a ground plane, was studied using laser-based particle image velocimetry and laser Doppler velocimetry. Measurements were made with nozzle pressure ratios of between 1.05 and 4 and nozzle height-to-diameter ratios of between 2.4 and 8.4, while nozzle spacing remained fixed at seven diameters. Mean fountain vertical velocity magnitude was observed to decrease with increasing nozzle height. Mean fountain upwash velocity profiles were found to be self-similar for all test conditions. A distinct frequency of fountain oscillation was identified but only at a nozzle height of 4.4 diameters.

Nomenclature

a_1	=	growth rate of fountain half-width [see Eq. (1)]
a_2	=	constant in Eq. (1)
D	=	nozzle exit internal diameter
H	=	nozzle exit height above the ground plane (see Fig. 1)
$\dot{M}$	=	fountain momentum flux
$\dot{M}_{\max}$	=	maximum fountain vertical momentum flux
R_f	=	radial distance from the fountain virtual origin (see Fig. 11)
r	=	radial distance from nozzle axis
S	=	distance between the nozzle centers (see Fig. 1)
U	=	time-mean velocity in the streamwise direction
$\hat{U}$	=	time-mean peak streamwise velocity in the fountain
U_j	=	time-mean jet centerline velocity at nozzle exit
$U_{\max}$	=	time-mean local maximum streamwise velocity in the fountain
u	=	instantaneous velocity in the streamwise direction (positive downward for jets; positive upward for fountains)
v	=	instantaneous velocity in the x direction
x	=	coordinate parallel to the ground plane in the plane of the jet centers (see Fig. 1)
$x_{0.5}$	=	fountain half-width where $U = U_{\max}/2$
x_1	=	fountain width
y	=	coordinate parallel to the ground plane in the plane of the nominal fountain axis (see Fig. 1)
z	=	coordinate normal to the ground plane (see Fig. 1)
θ	=	fountain included angle in the y–z plane (see Fig. 11)
$\lambda_{\dot{M}}$	=	fountain momentum flux ratio ($\dot{M}/\dot{M}_{\max}$)
ρ	=	air density

Presented as Paper 1402 at the 45th AIAA Aerospace Sciences Meeting and Exhibit, Reno, Nevada, 8–11 January 2007; received 4 June 2007; revision received 6 August 2007; accepted for publication 6 August 2007.

*Lecturer, Aeromechanical Systems Group, Defence Academy of the United Kingdom.

†Professor, Head of Aeromechanical Systems Group, Defence Academy of the United Kingdom. Associate Fellow AIAA.

‡Research Student, Aeromechanical Systems Group, Defence Academy of the United Kingdom.

Introduction

THE wall jets created by the impingement on the ground of the individual jet flows from a jet-lift, short takeoff and vertical landing (STOVL) aircraft, with two nozzles, meet at a stagnation line and form an upward-flowing "fountain" that interacts with the airframe (Fig. 1). In some cases this can provide a beneficial lift-generating ground cushion [1]. The fountain flow may also give rise to a variety of undesirable characteristics: hot gas ingestion; ground erosion; acoustic, thermal, and pressure loads on the airframe [2]. Despite many years of STOVL aircraft development, the unsteady nature of in-ground-effect aerodynamics remains poorly understood and continues to be of concern.

Early experimental work on fountain flows revealed that the use of a vertical reflection plane is inappropriate due to the interaction between the jets and the fountain [3]. Although the flow is generally symmetrical in the mean, instantaneous velocity fields show a high degree of asymmetry, the presence of large-scale vortical structures, and a stagnation region whose location is observed to vary randomly [4]. The fountain is quite sensitive to small imbalances between the jets [5,6] and appears to be unstable under certain conditions [7]. Further studies have reported turbulence intensities in the fountain upwash as high as 50% and a much greater rate of spreading in the fountain when compared to a freejet [8,9]. Velocities normal to the axis of the fountain upwash have been found to be in the region of 20–30% of the jet exit velocity, at least for incompressible experiments [9,10]. Positioning of the fountain is largely dependent upon the momentum ratio of the opposing wall jets with differences in their relative thicknesses causing the fountain to appear to lean [11]. Nozzle angle relative to the impingement plane or nozzle splay angle also plays an important part in the fountain location and development [10,11]. Visualization of multiple jet impingement has revealed the presence of large-scale coherent structures, evolving from the main jets, propagating through the wall jets, and dissipating in the fountain [12–15], with possible crossover of these structures from one wall jet to the opposite side of the fountain [16]. This may be responsible, in part, for the large degree of spreading associated with fountain flows.

Although it is evident that the fountain upwash flow is unsteady, only limited data on the transient characteristics of this flow region are available. Early experiments relied on intrusive measurement techniques to provide mean pressure data [7] with unsteady pressures on the ground plane being used to infer additional information [17]. Early attempts to acquire turbulence data used hot-wire anemometry [8,18], but this technique is limited to low flow speeds and low turbulence intensities and is therefore inaccurate for compressible and highly unsteady flows. Techniques such as particle image velocimetry (PIV) and laser Doppler velocimetry (LDV) offer the possibility of detailed nonintrusive measurements in the fountain

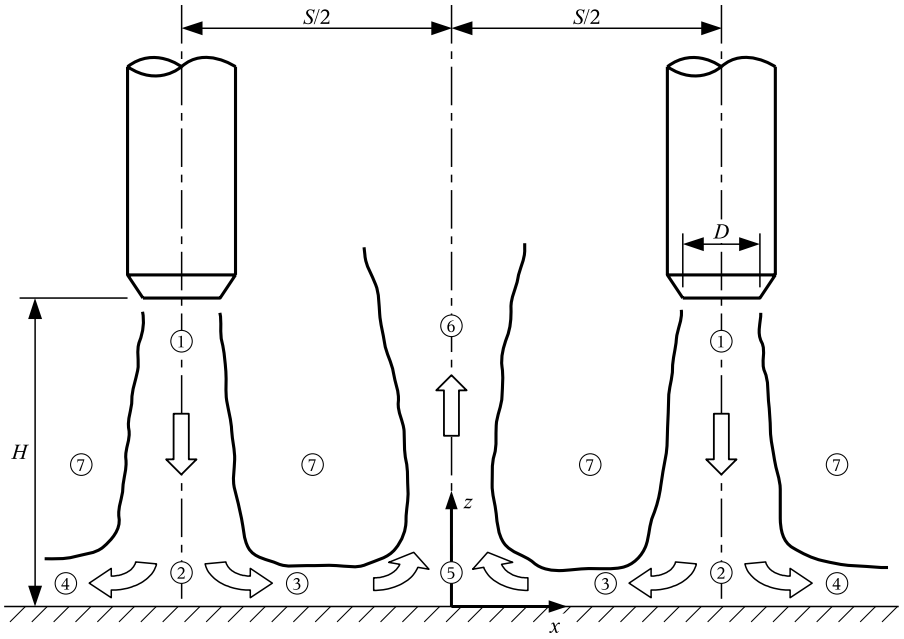

1. Lift jet flow
2. Jet impingement region
3. Inner wall jet flow
4. Outer wall jet flow
5. Fountain formation region
6. Fountain upwash flow
7. Entrainment region

Fig. 1 Schematic of a twin impinging jet fountain flow.

region. Previous investigations using these techniques have used water as the working fluid [9,10,19] or were limited to a single nozzle pressure ratio [20]. A combined examination of underexpanded impinging jets and fountain flows is necessary to understand the complete effect of NPR (the ratio of nozzle supply total pressure to ambient static pressure) on the development of the fountain. Recently we have reported on the mean impinging jet and fountain velocity profiles obtained using PIV [21]. This paper extends the work further in presenting specific fountain characteristics as well as transient behavior obtained using laser-based techniques.

Aims and Objectives

The continued development of STOVL aircraft, both manned and unmanned, with an increasing reliance on computational design techniques, is dependent upon a better understanding of the aerodynamics of jet-lift aircraft in ground effect. The aim of this work was to describe and quantify the fountain upwash flowfield (generated by a pair of impinging, turbulent, compressible jets) in the plane connecting the nozzle centerlines for a range of geometries and nozzle pressure ratios. The objectives of the work were as follows:

1) to analyze and quantify fountain spreading and decay;

2) to analyze and quantify any periodic "flapping" of the fountain flow.

Experimentation

Given that the fountain flow has been shown previously to be highly sensitive to small disturbances caused, for example, by probe interference, this study focused on nonintrusive measurements of the flowfield using PIV and LDV techniques.

Impinging Jet Facility

The experiments were conducted in a dedicated impinging jet facility. The test rig (Fig. 2) consisted of a small cylindrical settling chamber with an internal diameter of 230 mm and a height of 210 mm suspended from a $4 \times 4 \times 3$ m^3 steel frame. This rig was mounted in the center of a closed room measuring approximately $8 \times 8 \times 4$ m^3.

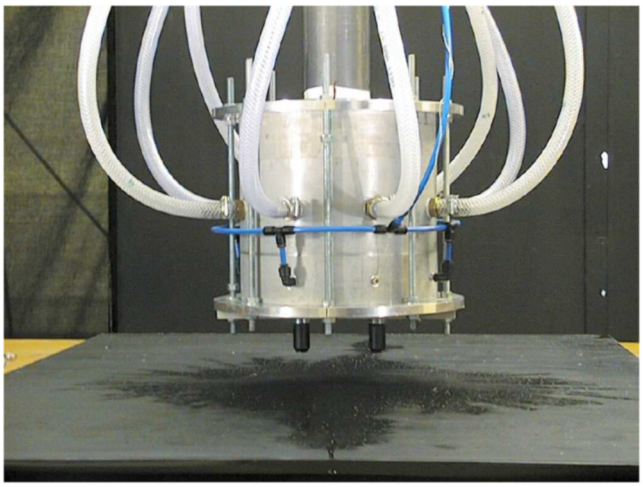

Fig. 2 The settling chamber and impingement surface.

The settling chamber has two internal screens and, on the lower surface, a replaceable nozzle-mounting plate that allows different configurations of nozzle spacing. Dried, ambient-temperature compressed air was supplied to the settling chamber through a 63.5 mm diam. flexible hose from two Howden screw-type compressors via a 34 m^3 storage tank. Maximum continuous flow rate was 0.9 kgs^{-1} and maximum pressure was 7 bar(g). The impingement surface consisted of a 1×1 m^2 aluminum plate placed on top of a 3×2 m^2 table. The nozzle settling chamber was instrumented with a *K*-type thermocouple and a Druck PDCR 10-3.5 pressure transducer that provided information on the stagnation temperature and pressure (via the small pressure lines seen in Fig. 2), respectively. Atmospheric pressure was measured using a SETRA 270 pressure transducer. The pressure in the settling chamber was adjusted using a CompAir A119 pneumatically controlled valve

driven by a computer and a current-to-pressure converter. The configuration used for the present study comprised two identical 63.5-mm-long axisymmetric convergent nozzles with an exit diameter D of 12.7 mm (following the "short half-inch" nozzle design used by Bray [22]) and a nozzle spacing S of seven diameters. The jets were seeded by JEM Hydrosonic long-lasting fluid droplets (≈ 1 μm diam) generated by a TSI 9306 Six-Jet atomizer connected to a Clarke compressor and injected through eight ports in the settling chamber (the large pressure lines seen in Fig. 2). The ambient air was seeded with smoke particles produced by a Le Maitre Turbo Mist fog generator. The uncertainty in the pressure control system was estimated to be $\pm 0.5\%$ of NPR [23].

Particle Image Velocimetry

The PIV equipment consisted of a New Wave Gemini II Nd:YAG double-pulsed laser that, through the use of a combination of plano-concave and plano-cylindrical lenses, created a light sheet approximately 1 mm thick, positioned perpendicular to the impingement plane and passing through the plane defined by the nozzle axes. The PIV double-pulsed image pairs were acquired using a Kodak Megaplus ES1.0 digital camera with a resolution of 1016×1008 pixels at a rate of 15 image pairs per second. The camera was fitted with a 60 mm, f2.8 Nikon lens and placed normal to the light sheet at a distance of approximately 550 mm. This provided a maximum field of view of 82×83 mm^2 ($6.4D \times 6.5D$). It was assumed that the maximum velocity in the upwash fountain was around half the maximum jet velocity (assuming isentropic conditions), and the maximum out-of-plane velocity was 25% of the fountain upwash velocity. This resulted in a pulse separation of between 2.6 μm (NPR = 4) and 6.6 μm (NPR = 1.05).

Approximately 500 PIV image pairs were acquired per test case. Data from each image pair consisted of instantaneous streamwise u, and cross stream v, velocities in the z and x directions, respectively. The commercial software Insight v3.3 by TSI was used to process the images. A fast Fourier transform cross-correlation algorithm was used to extract the velocity vectors. Interrogation windows of 32×32 pixels with 75% overlapping were employed in the processing. The size of the interrogation window was chosen to allow for a minimum of 10 seeding particles per interrogation area and to allow for the maximum in-plane particle displacement to be less than one-quarter of the size of the interrogation window. Inherent to PIV processing are the spurious vectors which, on average, accounted for less than 3% of the total. Images that generated velocity vector fields with spurious vectors of more than 3 standard deviations from the data set mean were rejected (approximately 5%). For those velocity vector fields that were not rejected, spurious vectors were filtered using a bandpass filter followed by a local median filter. The resulting empty spaces were filled with interpolated values from the surrounding area. The uncertainty in the measured velocity using PIV was estimated to be $\pm 3\%$ [23].

Laser Doppler Velocimetry

LDV measurements were made using a Dantec FibreFlow system operating in backscatter mode. This consisted of a 4 W Lexel Model 95, water-cooled, argon-ion laser, a Dantec 60×41 transmitter with 60×24 fiber optic manipulators, Dantec 57N20 burst spectrum analyzer, a Dantec 2-D FiberFlow probe and a 1 m focal length lens with a 2× beam expander. The lens and beam expander combination created a measurement volume of $0.15 \times 4.2 \times 0.15$ mm^3. Bragg shifting by 40 MHz was used for directional discrimination. Alignment was completed using a 35 μm pinhole with a photovoltaic cell. Data processing included the filtering of any data outside 3 standard deviations from the mean. Mean and rms velocities were calculated using a weighted average technique. Each measurement point consisted of around 100,000 samples. The irregular time-spaced LDV data were resampled at regular intervals at twice the mean data rate using a nearest-neighbor resampling technique. The resampled data were divided into segments of 2^{13} samples and processed using the Welch method and a Hanning window to reduce the spectral leakage. The uncertainty in the measured velocity using LDV was estimated to be $\pm 9\%$ [23].

Results

Results are presented for PIV and LDV measurements made under the following conditions:

1) a nozzle spacing-to-diameter ratio, S/D, of 7;
2) nozzle height-to-diameter ratios H/D of 2.4, 4.4, 6.4, and 8.4;
3) NPRs of 1.05, 2, 3, 3.25, 3.5, 3.75, and 4.

LDV data were acquired along a line joining the nozzle centerlines at heights above the ground of $z/D = 0.5$, $z/D = 1$, and $z/D = 2$.

Mean Flowfield

The fountain has been shown to be very sensitive to small variations in the generating jets, ground plane angle, and even in the environment surrounding the experimental facilities [6]. Throughout the experiments the jets were generated by the same pair of nozzles, the ground plane was unvarying, and the surrounding environment was similar. It was important, therefore, to check that the two jets had as near identical characteristics as possible. Figure 3 shows an example of LDV-measured velocity and turbulence intensity profiles $0.1D$ downstream of the nozzle exit plane, in this case at an NPR of 3.

The velocity profiles (Fig. 3a) are virtually identical with a maximum difference between the left and right jets of 0.8%, which is well within the bounds of measurement uncertainty. The velocity profile exhibits a velocity deficit toward the centerline. This is characteristic of the curvature of the sonic line at the nozzle exit and typical of underexpanded jets issuing from convergent nozzles [24]. Peak turbulence intensity (Fig. 3b) in the jet shear layer was in the region of 10%, while on the jet centerline 3% was typical. Both jets have turbulence intensity profiles that, within the limits of measurement uncertainty, are in agreement. Despite the care taken to ensure the jet flows were as near identical as possible, the fountain

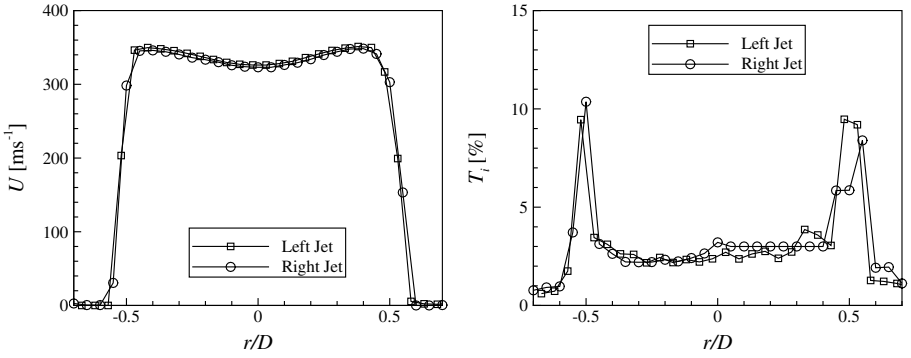

a) Axial velocity **b) Turbulence intensity**

Fig. 3 LDV-measured velocity and turbulence intensity profiles $0.1D$ downstream of the nozzle exit plane (NPR = 3).

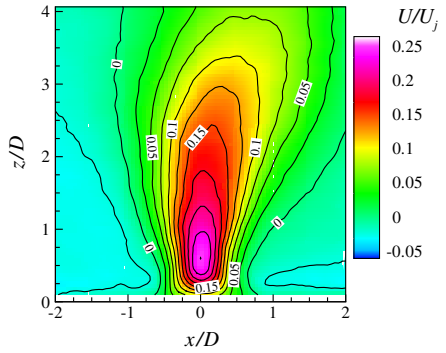

Fig. 4 PIV-measured time-averaged vertical velocity, U/U_j (NPR = 1.05, $S/D = 7$, and $H/D = 4.4$).

was found to lean relative to the vertical axis, although not consistently in one particular direction. In general, and with few exceptions, this phenomenon was shown to occur under the majority of the conditions tested.

The fountain flow is characterized by a region of high vertical velocity before it starts to decay. Figure 4 shows contours of mean vertical velocity for $H/D = 4.4$ and NPR = 1.05. The fountain can be defined as a narrow region ($\approx 0.5D$ wide) extending from $z/D \approx 0.3D$ up to $z/D \approx 1.5$. Peak vertical velocity, of approximately 22 ms^{-1} (i.e., $\approx 0.25U_j$), is attained up to $z/D \approx 1$. The vertical velocity of the fountain flow is dependent on the peak velocity in the wall jet, which at more than three nozzle diameters away from the nozzle axis is independent of nozzle height for this low pressure ratio [25]. At higher pressure ratios, the flowfield, although broadly similar in structure, did exhibit some dependency on nozzle height.

Vertical velocity profiles, when nondimensionalized with the local maximum mean fountain upwash velocity U_{max} and fountain half-width $x_{0.5}$, were found to be largely self-similar above the fountain formation region for all nozzle heights and pressure ratios tested. An example is shown in Fig. 5 for $H/D = 4.4$.

Velocity Decay

The effect of nozzle height and pressure ratio on the peak vertical velocity in the fountain $\hat{U}$ is shown in Fig. 6. ($\hat{U}$ is the highest measured vertical velocity in the fountain, whereas U_{max} is the highest measured vertical velocity in the fountain at a specific height above the impingement plane.) At NPR = 1.05 and NPR = 2 the peak upwash velocity was shown to be largely independent of nozzle height, as was the height at which this peak vertical velocity occurs (Fig. 7). With further increase in NPR the peak upwash velocity

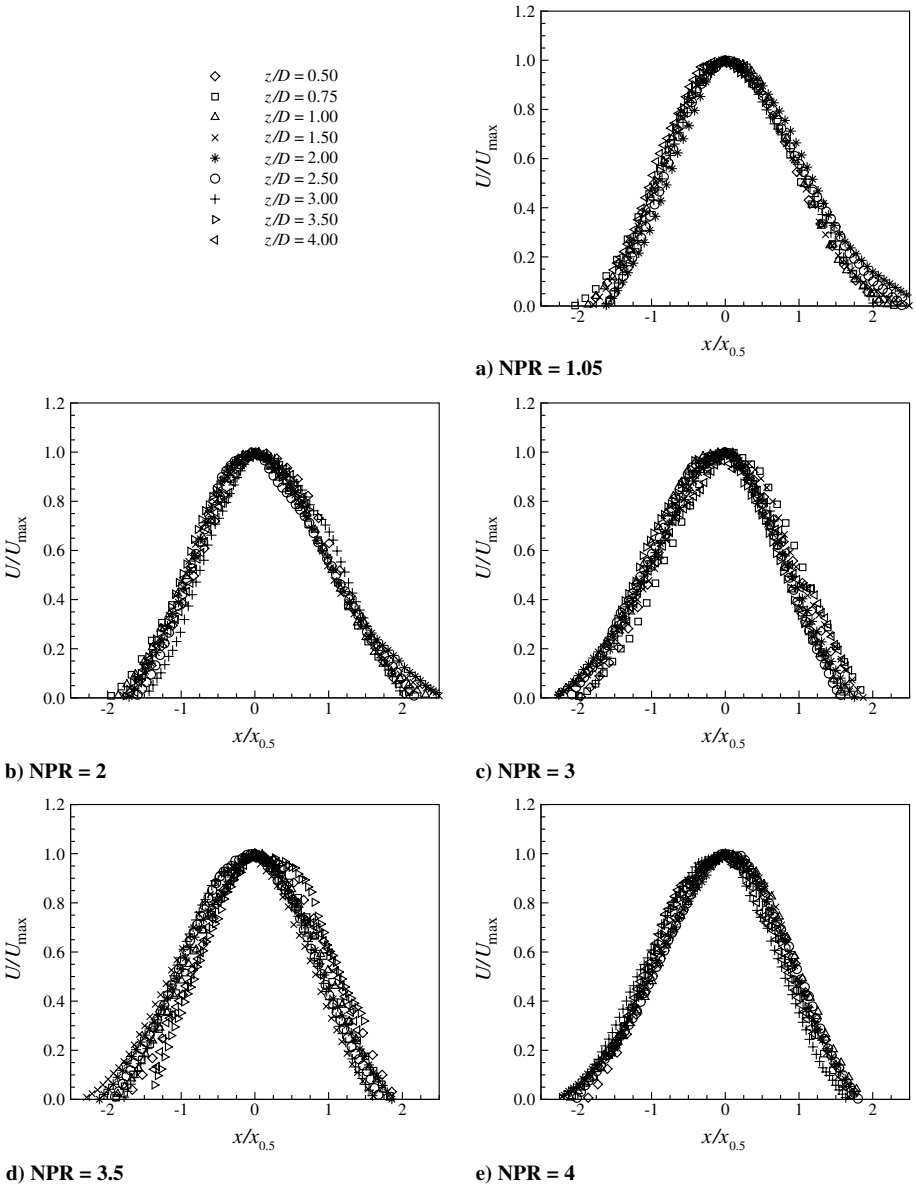

Fig. 5 PIV-measured nondimensional mean vertical velocity profiles ($H/D = 4.4$, $S/D = 7$).

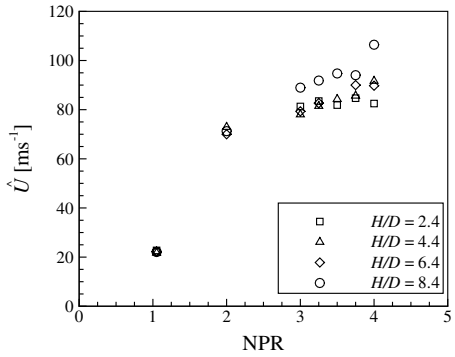

Fig. 6 PIV-measured mean peak fountain vertical velocity, $\hat{U}$ ($S/D = 7$).

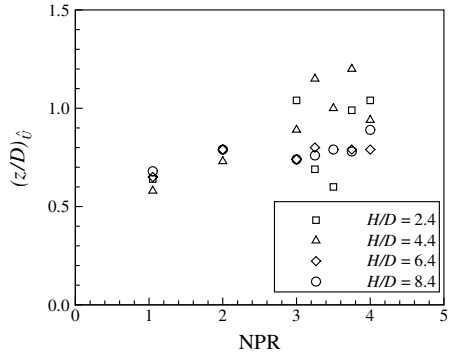

Fig. 7 PIV-derived height of fountain mean peak vertical velocity ($S/D = 7$).

shows a gradual increase and is relatively unaffected by nozzle height up to $H/D = 6.4$; however, the position of peak vertical velocity varies nonmonotonically with NPR at $H/D = 2.4$ and $H/D = 4.4$. These discontinuities in the position of maximum vertical velocity are due to changes in the shock-cell structure of the jet flow in the impingement region. At $H/D = 6.4$ and $H/D = 8.4$, these differences are not as marked as for lower nozzle heights, resulting in a smaller variation of the position of peak vertical velocity in the fountain.

Downstream of the position of peak vertical velocity (increasing z/D) the vertical velocity in the fountain was found to decrease with increasing height above the impingement plane. Furthermore, increasing nozzle height resulted in a slower decay of vertical velocity. Figure 8 shows the rate of decay of fountain velocity $[\mathrm{d}(U_{\max}/U_j)/\mathrm{d}(z/D)]$, where higher decay rates are more negative values, for all the nozzle configurations tested. At the two lowest NPRs the decay of maximum fountain vertical velocity is similar (within 7%) showing a quasi-linear variation with nozzle height. The variation of decay rate with NPR exhibits a similar development for all the nozzle heights, with a nearly constant decay between NPR = 1.05 and NPR = 2. The slowest decay rates occurred in the region of $3 \leq \mathrm{NPR} \leq 3.25$. Further increase in nozzle pressure ratio resulted in a higher rate of decay. For NPR ≥ 3, configurations with $H/D = 2.4$ were found to decay at a significantly lower rate than was observed to occur at higher H/D.

Spreading Rate

The growth of fountain half-width with height above the ground for varying H/D at NPR = 3 is shown in Fig. 9. Spreading of the fountain increases approximately linearly with nozzle height above the ground. The fountain's growth rate (or spreading rate), the variation of $x_{0.5}$ with distance from the impingement plane, can be represented by

$$\frac{x_{0.5}}{D} = a_1\left(\frac{z}{D}\right) + a_2 \tag{1}$$

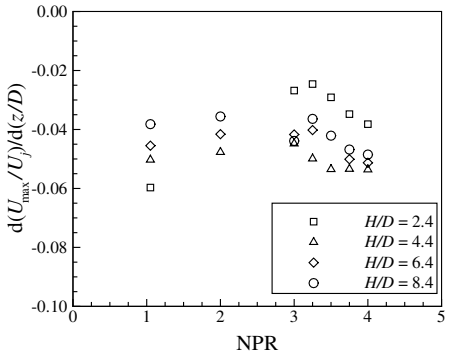

Fig. 8 PIV-derived rate of mean fountain vertical velocity decay ($S/D = 7$).

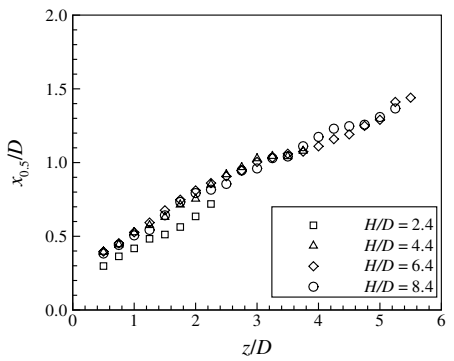

Fig. 9 PIV-derived growth of fountain half-width (NPR = 3, $S/D = 7$).

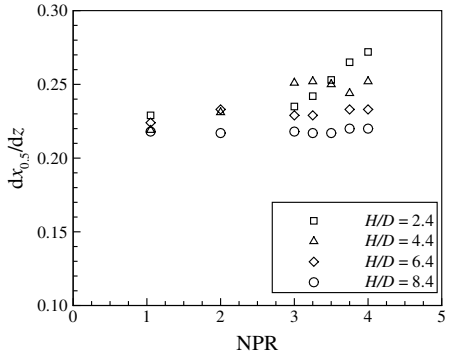

Fig. 10 PIV-derived growth rates of fountain half-width ($S/D = 7$).

where a_1 is the growth rate of the fountain half-width, and a_2 is the half-width at $z = 0$. Growth rates were observed to be largely independent of nozzle height for NPR = 1.05 with growth rates, $\mathrm{d}x_{0.5}/\mathrm{d}z$, of between 0.22 and 0.23 (Fig. 10). With underexpanded jet conditions, the spreading of the fountain was shown to have a dependency on both nozzle pressure ratio and nozzle height. This seems likely to be an effect of modifications to the jet shock structure as these parameters are changed. At $H/D = 2.4$, the spreading rate increased monotonically with increasing NPR. At the higher values of H/D (6.4 and 8.4) the variation of the spreading rate with NPR showed a similar trend, albeit with a significantly diminished slope. At $H/D = 4.4$ a different result was observed: for NPRs of 2, 3, 3.25, and 3.5, the spreading rate was higher than expected based on the trend discussed above. These height and NPR combinations correlate with the identification of a characteristic frequency in the fountain spectra (discussed later in this paper). The enhanced spreading rate observed at $H/D = 4.4$ may be indicative of the existence of a feedback mechanism, possibly similar to that observed in a single impinging jet, and appears stronger at particular heights and less

prominent at others. Krothapalli et al. [26] suggest that in single impinging jets the feedback mechanism is due to the reflection of acoustic waves that travel back to the jet exit.

Momentum Flux Ratio

The fountain half-width and velocity decay have been shown to have approximately linear variations with height above the impingement plane. This does not, however, give any indication regarding the fountain's vertical momentum. Fountain vertical momentum flux ratio, the ratio of vertical momentum flux in the fountain at a given height to the maximum vertical momentum flux, was defined as

$$\lambda_{\dot{M}} = \frac{\dot{M}}{\dot{M}_{\max}} \tag{2}$$

Based on the observations of Abbott and White [6], the fountain was assumed to spread in a circular arc in the y–z plane through a constant angle, θ. Figure 11 shows an idealized view of the twin impinging jet experiment viewed along the positive x axis. The solid black lines indicate a notional fountain boundary while the arrows indicate flow direction. The virtual origin of the fountain was determined by fitting Eq. (1) to the values of the spreading rate of the fountain, setting $x_{0.5} = 0$ and solving for z/D. Hence,

$$\frac{R_f}{D} = -\frac{a_2}{a_1} + \frac{z}{D} \tag{3}$$

where R_f is the radial distance from the virtual origin of the fountain upwash to the measurement point of interest (Fig. 11). The fountain momentum flux $\dot{M}$ may then be determined as

$$\dot{M} = \rho R_f \theta \int_{-x_1}^{x_1} U^2 \mathrm{d}x \tag{4}$$

where ρ is the fluid density in the fountain and x_1 is the fountain width. Equation (4) may be rewritten as

$$\dot{M} = \rho \frac{R_f}{D} D\theta x_{0.5} U_{\max}^2 \int_{-x_1/x_{0.5}}^{x_1/x_{0.5}} \left(\frac{U}{U_{\max}}\right)^2 \mathrm{d}(x/x_{0.5}) \tag{5}$$

and hence,

$$\lambda_{\dot{M}} = \frac{\rho \frac{R_f}{D} D\theta x_{0.5} U_{\max}^2 \int_{-x_1/x_{0.5}}^{x_1/x_{0.5}} (\frac{U}{U_{\max}})^2 \,\mathrm{d}(x/x_{0.5})}{\{\rho \frac{R_f}{D} D\theta x_{0.5} U_{\max}^2 \int_{-x_1/x_{0.5}}^{x_1/x_{0.5}} (\frac{U}{U_{\max}})^2 \,\mathrm{d}(x/x_{0.5})\}_{\max}} \tag{6}$$

From Fig. 5, however, it was shown that the vertical velocity profiles, when nondimensionalized with the local maximum mean fountain upwash velocity $U_{\max}$ and fountain half-width $x_{0.5}$, were self-similar above the fountain formation region for all nozzle heights and pressure ratios tested. Equation (6) may, therefore, be approximated to

$$\lambda_{\dot{M}} = \frac{(\frac{-a_2}{a_1} + \frac{z}{D}) x_{0.5} U_{\max}^2}{\{(\frac{-a_2}{a_1} + \frac{z}{D}) x_{0.5} U_{\max}^2\}_{\max}} \tag{7}$$

Maximum momentum flux in the fountain [proportional to the denominator of Eq. (7)] is shown in Fig. 12. Both nozzle height and NPR have a significant influence on the peak momentum flux in the fountain for underexpanded jet conditions. Wall-jet momentum flux has been reported to increase with nozzle height [27,28]; it is not surprising, therefore, that fountain momentum flux behaves in a similar manner. The increase in peak momentum flux ratio with increasing NPR is largely dominated by the square term of maximum vertical velocity since the fountain's half-width at the height of peak momentum flux is approximately constant ($x_{0.5} \approx 1D$).

The vertical distribution of the momentum flux ratio is shown in Fig. 13. NPR appears to have little effect; however, increasing nozzle height causes the fountain momentum flux ratio to spread over a greater vertical distance. The height of maximum momentum flux

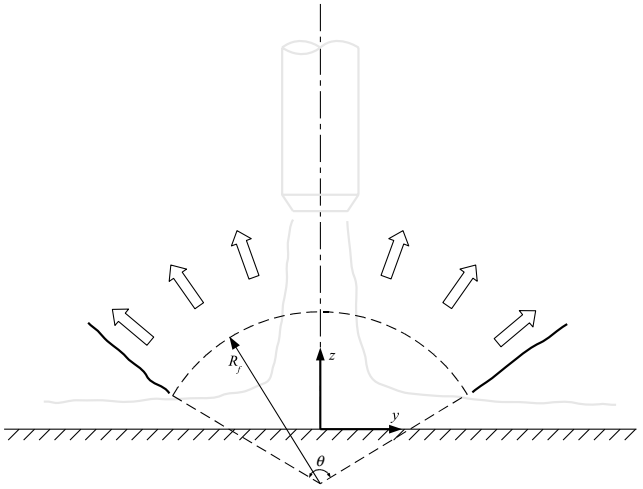

Fig. 11 Side view of the twin impinging jet experiment at $x = 0$ showing the idealized fountain spreading. Open arrows indicate nominal fountain flow direction in the y–z plane; a nominal fountain edge is shown (analagous to the freejet and wall-jet boundaries of Fig. 1); the extent of the fountain in the y–z plane is indicated by θ; R_f is the fountain radial coordinate from its virtual origin.

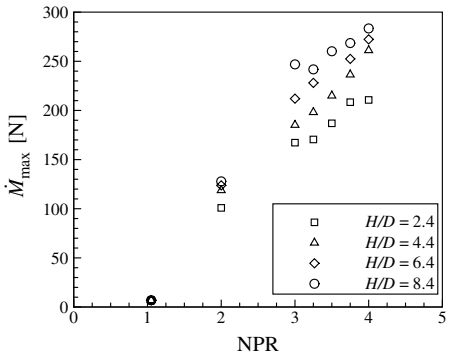

Fig. 12 Maximum momentum flux in the fountain.

was observed to occur at around $2.25 \leq z/D \leq 3$ after which the momentum flux decreases due to viscous mixing.

Power Spectral Density

The increased level of spreading observed in the fountain when compared to normal jet development may, in part, be due to the oscillation of the flow, resulting in a fountain that appears to spread more than its instantaneous structure would suggest. Further study would be needed to establish whether this is an acoustically induced phenomenon of the type reported by Krothapalli et al. [26]. It is evident that the fountain upwash is unsteady; however, the data rate of the PIV system did not permit the quantification of transient features of this flow region. The high data rate LDV measurements address this issue, capturing the smaller-scale high-frequency components of the upwash oscillation. The data gathered showed that the majority of the horizontal turbulent energy in the upwash is contained within the first 600 Hz of the frequency spectra, decaying with further increases in frequency. The slope of the decay of horizontal turbulent energy followed the $-5/3$ spectral law [29]. For $H/D = 2.4$, 6.4, and 8.4 the spectra showed a similar pattern, with increasing horizontal energy for increasing NPR and decreasing z/D; however, at $H/D = 4.4$ the frequency distribution of the horizontal energy displayed a pattern not observed at other nozzle heights. At this nozzle height and for underexpanded jet conditions only, the power spectral density (PSD) distribution had a distinct peak. The frequency at which the peak occurred was observed to increase with increasing NPR. Figures 14 and 15 show that the peaks

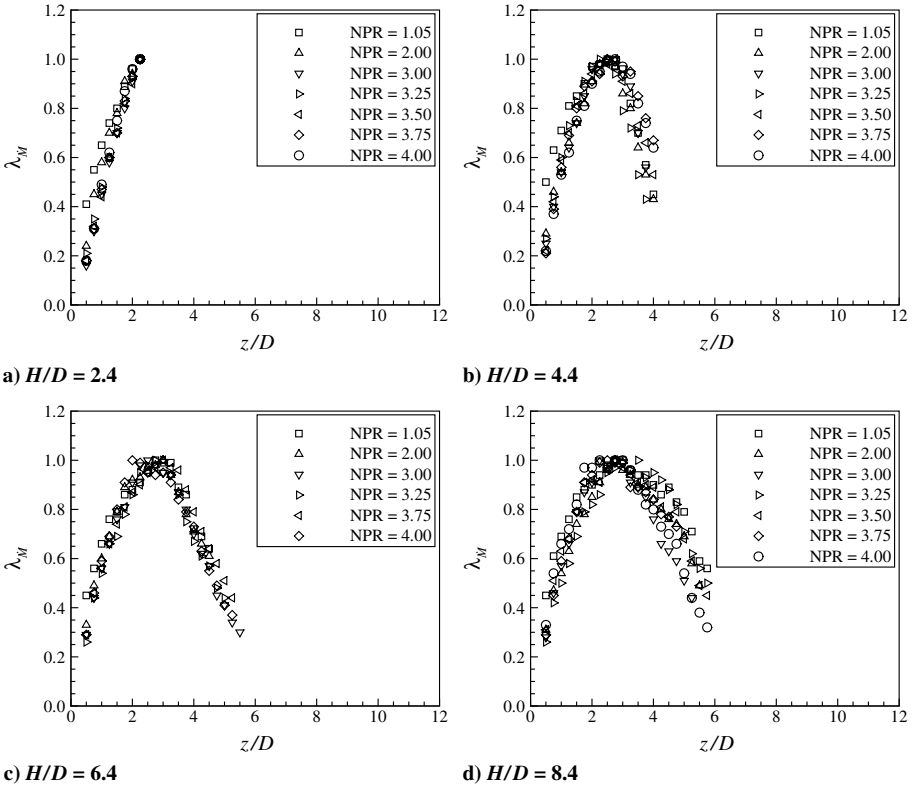

Fig. 13 Momentum flux ratio through the fountain.

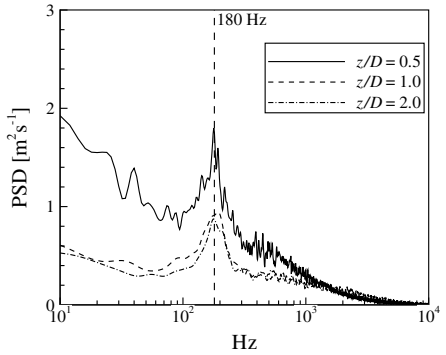

Fig. 14 LDV-derived power spectral density peaks (NPR = 2.0, H/D = 4.4, and S/D = 7).

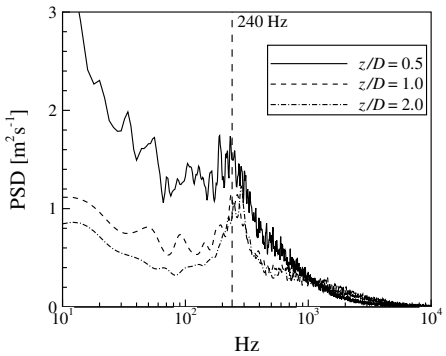

Fig. 15 LDV-derived power spectral density peaks (NPR = 3.0, H/D = 4.4, and S/D = 7).

in the power spectral distribution occur at 180 and 240 Hz for NPR = 2 and NPR = 3, respectively. At NPR = 4 (Fig. 16) no distinct peak was observed, although a broadband "hump" was identified at 300 Hz for $z/D = 1$ and $z/D = 2$. The fact that the

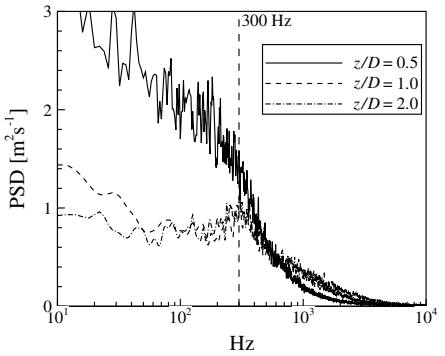

Fig. 16 LDV-derived power spectral density peaks (NPR = 4.0, H/D = 4.4, and S/D = 7).

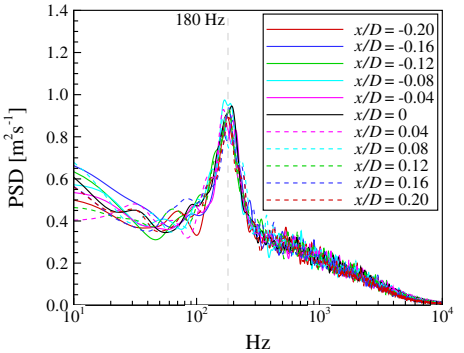

Fig. 17 LDV-derived power spectral density peaks for varying horizontal position (NPR = 2, H/D = 4.4, S/D = 7, and z/D = 1).

frequency of the peaks does not change with varying horizontal position (Fig. 17) implies that under the particular test conditions the distribution of horizontal energy is dominated by large-scale structures (with dimensions of at least $0.4D$) rather than by the small scales of turbulence.

Conclusions

An experimental investigation has been conducted on the fountain flowfield formed by the collision of wall jets created by two axisymmetric, high-speed, turbulent, compressible jets. Mean fountain characteristics for nozzle pressure ratios of between 1.05 and 4 and nozzle height-to-diameter ratios of 2.4, 4.4, 6.4, and 8.4 were acquired. The nozzle spacing remained fixed at seven diameters. Fountain local maximum vertical velocity was observed to decrease with increasing height above the ground. The rate of decrease was dependent upon the nozzle pressure ratio. Fountain half-width was observed to increase linearly with height above the ground independent of nozzle height and pressure ratio. Mean fountain vertical velocity was found to be self-similar across the range of test conditions and is therefore independent of nozzle height and pressure ratio. This self-similarity allowed the calculation of momentum flux ratio and showed that peak momentum flux ratio is obtained at a similar height above the ground over the range of nozzle heights and pressure ratios quoted. The fountain spectral measurements showed a distinct frequency of horizontal oscillations. This frequency was only observed in the spectra with underexpanded jets and for a nozzle height-to-diameter ratio of 4.4 and correlated with increased spreading rates of the fountain.

Acknowledgments

This work was partly funded by the Engineering and Physical Sciences Research Council under Grant GR/R42894/01, and their support is gratefully acknowledged.

References

[1] Anderson, S. B., "Jet-Powered V/STOL Aircraft—Lessons Learned," *International Powered Lift Conference and Exhibit*, RAeS, London, England, U.K., 29–31 Aug. 1990, pp. II.1.1–II.1.14.

[2] Curtis, P., "A Review of the Status of Ground Effect/Environment Technologies," AIAA Paper 2002-5985, 5–7 Nov. 2002.

[3] Margason, R. J., "Review of Propulsion-Induced Effects on Aerodynamics of Jet/STOL Aircraft," NASA, TN D-5617, 1970.

[4] Saddington, A. J., Cabrita, P. M., and Knowles, K., "Large-Scale Instabilities in a STOVL Upwash Fountain," *Engineering Turbulence Modelling and Experiments 6*, edited by W. Rodi and M. Mulas, Elsevier Science Ltd., Oxford, U.K., 2005, pp. 667–676, ISBN 0 08 044544 6.

[5] Skifstad, J. G., "Aerodynamics of Jets Pertinent to VTOL Aircraft," *Journal of Aircraft*, Vol. 7, No. 3, 1970, pp. 193–204.

[6] Abbott, W. A., and White, D. R., "The Effect of Nozzle Pressure Ratio on the Fountain Formed Between Two Impinging Jets," RAE, TM P1166, 1989.

[7] Hall, G. R., and Rogers, K. H., "Recirculation Effects Produced by a Pair of Heated Jets Impinging on a Ground Plane," NASA, Contractor Rept. CR-1307, 1969.

[8] Gilbert, B. L., "Turbulence Measurements in a Radial Upwash," *AIAA Journal*, Vol. 27, No. 1, Jan. 1989, pp. 44–51.

[9] Barata, J. M. M., "Fountain Flows Produced by Multi-Jet Impingement on a Ground Plane," *Journal of Aircraft*, Vol. 30, No. 1, 1993, pp. 50–56.

[10] Behrouzi, P., and McGuirk, J. J., "Experimental Data for CFD Validation of Impinging Jets in Cross-Flow with Application to ASTOVL Flow Problems," *Conference Proceedings Fluid Dynamics Panel Symposium*, CP-534, AGARD, 19–22 April 1993.

[11] Siclari, M. J., Hill, W. G., and Jenkins, R. C., "Stagnation Line and Upwash Formation of Two Impinging Jets," *AIAA Journal*, Vol. 19, No. 10, Oct. 1981, pp. 1286–1293.

[12] Wohllebe, F. A., and Siclari, M. J., "Fountain and Upwash Flowfields of Multijet Arrangements," *Journal of Aircraft*, Vol. 15, No. 8, Aug. 1978, pp. 468–473.

[13] Saripalli, K. R., "Visualization of Multijet Impingement Flow," *AIAA Journal*, Vol. 21, No. 4, April 1983, pp. 483–484.

[14] Kibens, V., Saripalli, K. R., Wlezien, R. W., and Kegelman, J. T., "Unsteady Features of Jets in Lift and Cruise Modes for VTOL Aircraft," *International Powered Lift Conference and Exhibit*, Society of Automotive Engineers, Warrendale, PA, 7–10 Dec. 1987, pp. 543–552; also Paper 872359.

[15] Cabrita, P. M., Saddington, A. J., and Knowles, K., "Unsteady Features of Twin-Jet STOVL Ground Effects," AIAA Paper 2002-6014, 5–7 Nov. 2002.

[16] Childs, R. E., and Nixon, D., "Turbulence and Fluid/Acoustic Interaction in Impinging Jets," *International Powered Lift Conference and Exhibit*, Society of Automotive Engineers, Warrendale, PA, 7–10 Dec. 1987, pp. 447–458; also Paper 872345.

[17] Knowles, K., Wilson, M. J., and Bray, D., "Unsteady Pressures Under Impinging Jets in Cross-Flows," *AIAA Journal*, Vol. 31, No. 12, 1993, pp. 2374–2375.

[18] Kotansky, D. R., and Glaze, L. W., "The Effects of Ground Wall-Jet Characteristics on Fountain Upwash Flow Formation and Development," AIAA Paper 81-1294, 23–25 June 1981.

[19] El-Okda, Y., and Telionis, D. P., "Experimental Investigation of Twin Jet Impinging on the Ground With and Without a Free Stream," AIAA Paper 2002-5976, 5–7 Nov. 2002.

[20] Elavarasan, R., Venkatakrishnan, L., Krothapalli, A., and Lourenço, L., "Supersonic Twin Impinging Jets," AIAA Paper 2000-0812, 10–13 Jan. 2000.

[21] Cabrita, P. M., Saddington, A. J., and Knowles, K., "PIV Study of a Twin-Jet STOVL Fountain Flow," *The Aeronautical Journal*, Vol. 109, No. 1100, Oct. 2005, pp. 439–449.

[22] Bray, D., "Jets in Cross-Flow and Ground Effect," Ph.D. Thesis, Cranfield Institute of Technology, Shrivenham, U.K., 1992.

[23] Cabrita, P. M., "Steady and Unsteady Features of Twin-Jet STOVL Ground Effects," Ph.D. Thesis, Cranfield University, Shrivenham, U.K., 2006.

[24] Saddington, A. J., Lawson, N. J., and Knowles, K., "An Experimental and Numerical Investigation of Under-Expanded Turbulent Jets," *The Aeronautical Journal*, Vol. 108, No. 1081, March 2004, pp. 145–152.

[25] Myszko, M., and Knowles, K., "Turbulence Measurements in RadialWall Jets," *Experimental Thermal and Fluid Science*, Vol. 17, Nos. 1–2, 1998, pp. 71–78. doi:10.1016/S0894-1777(97)10051-6

[26] Krothapalli, A., Rajakuperan, E., Alvi, F. S., and Lourenço, L., "Flow Field and Noise Characteristics of a Supersonic Impinging Jet," *Journal of Fluid Mechanics*, Vol. 392, Aug. 1999, pp. 155–181. doi:10.1017/S0022112099005406

[27] Myszko, M., and Knowles, K., "Development of a Wall Jet from an Impinging, Round, Turbulent, Compressible Jet," AIAA Paper 94-2327, 20–23 June 1994.

[28] Myszko, M., "Experimental and Computational Studies of Factors Affecting Impinging Jet Flowfields," Ph.D. Thesis, Cranfield University, Shrivenham, U.K., 1997.

[29] Tennekes, H., and Lumley, J. L., *A First Course in Turbulence*, MIT Press, Cambridge, MA, 1972.